Two-dimensional MoSi₂N₄: An Excellent 2D Semiconductor for Field-Effect Transistors

Keshari Nandan, *Graduate Student Member, IEEE*, Barun Ghosh, Amit Agarwal, Somnath Bhowmick, and Yogesh S. Chauhan, *Fellow, IEEE*

Abstract—We report the performance of field-effect transistors (FETs), comprised of mono-layer of recently synthesized layered two-dimensional MoSi₂N₄ as channel material, using the first principles quantum transport simulations. The devices' performance is assessed as per the International Roadmap for Devices and Systems (IRDS) 2020 roadmap for the year 2034 and compared to advanced silicon-based FETs, carbon nanotube-based FETs, and other promising two-dimensional materials based FETs. Finally, we estimate the figure of merits of a combinational and a sequential logic circuit based on our double gate devices and benchmark against promising alternative logic technologies. The performance of our devices and circuits based on them are encouraging, and competitive to other logic alternatives.

Index Terms—Field-effect transistors (FETs), Density functional Theory (DFT), Maximally-localised Wannier functions (MLWF), Non-equilibrium Greens function (NEGF), Quantum Transport (QT), Mono-layer (ML).

I. Introduction

THE two-dimensional (2D) semiconductors are promising channel materials for future technology nodes, owing to the ultrathin thickness (< 1 nm), no surface dangling bonds, and sharp turn-on of the density of states (DOS) at band edges [1]–[4]. In the last five years, there has been remarkable progress on synthesizing novel 2D semiconductors and several promising device concepts [5]–[7] have been demonstrated based on them. Also, the shortest MoS₂ transistor with 1 nmgate length has been fabricated, which shows a near-ideal subthreshold swing of $\sim 65\,\mathrm{mV/decade}$ and an ON/OFF current ratio of $\sim 10^6$ [8].

The 2D semiconductors materials library has been enriched due to their bulk, arranged in layered form, in which intralayers bonds are strong covalent bonds and weak Van der Walls (vdW) force connects inter-layers. Advanced experimental techniques have been used to isolate their layers from bulk. But, most bulk materials are non-layered (strong covalent bonds connect all three dimensions). Thus, the exfoliation process can not create their 2D structure. Recently, Silicon has been introduced as a passivator during the CVD growth of non-layered molybdenum nitride (MoN₂) [9]. This process

This work was supported in part by the Humboldt Foundation and in part by the Swarnajayanti Fellowship (Grant No. – DST/SJF/ETA-02/2017-18) of the Department of Science and Technology (DST), Government of India.

results in the growth of the centimeter-scale film of layered 2D MoSi₂N₄.

Mono-layer (ML) MoSi₂N₄ has excellent mechanical, electronic, optical, and thermal properties [9]-[13]. It is also a promising photocatalyst for water splitting and CO2 reduction [10], [12]. It has been shown that ML-MoSi₂N₄ has excellent stability (far better than other 2D semiconductors), using phonon, molecular dynamics (MD) calculations, and experimental testing. Even it can be handled, processed, and stored without any protective environment, unlike black phosphorus (In ambient conditions, black phosphorus (BP) can be easily etched due to chemical degradation [14]) and MoS₂ (In moist air below 373 K, its surface starts oxidizing [15]). The Young's modulus and breaking strength for ML-MoSi₂N₄ are $\sim 479\,\mathrm{GPa}$ and $\sim 49\,\mathrm{GPa}$, respectively. These values are more than double of ML-MoS₂. ML-MoSi₂N₄ is an indirect band gap semiconductor with the experimental band gap value of $1.94\,\mathrm{eV}$. Its elastic constant is ~ 4 times of ML-MoS₂, and the carrier mobilities in it are ~ 4 times and $\sim 4\text{-}6$ times of ML-MoS₂ (the most widely studied 2D material for FETs application [8], [16]–[28]). Its lattice thermal conductivities [11], [12] are approximately 1.6 times silicon (Si) and much higher than other widely known 2D semiconductors [29]-[31] (ML-MoS₂, As, Sb, silicene and, ML-BP), but much lower than graphene [29], [32]. The high lattice thermal conductivity of ML-MoSi₂N₄ ensures a high rate of heat removal through nano-electronic devices comprised of this material. Its optical transmittance is high ($\sim 97 \%$) and comparable to graphene. The metal contacts to the ML of MoSi₂N₄ show exceptional physical properties with a large Schottky barrier height slope parameter, outperforming most other 2D semiconductors. CMOS compatible metals (Sc and Ti) also show excellent ohmic contact to ML-MoSi₂N₄ with zero interfacial tunneling barrier [33], [34]. Overall, Mono-layer MoSi₂N₄ is an excellent semiconductor for logic applications. However, there is a need to investigate the transport properties of FETs based on ML-MoSi₂N₄, and performance of integrated circuits (ICs) comprised of MoSi₂N₄ FETs.

Here, we exploit the capabilities of maximally localized Wannier functions (MLWFs) [35]–[37] to model electronic structure of ML-MoSi₂N₄ and generate tight-binding (TB) like Hamiltonian for the targeted device dimensions. Next, we compute transport properties of n- and p-type devices based on this ML by solving coupled Poisson and Schrödinger equations in non-equilibrium Green's functions (NEGF) formalism. We assess the performance of MoSi₂N₄ based FETs as per the requirements of International Roadmap for Devices and

K. Nandan and Y. S. Chauhan are with the NanoLab, Department of Electrical Engineering, Indian Institute of Technology Kanpur, India, 208016, e-mail: keshari@iitk.ac.in, chauhan@iitk.ac.in.

B. Ghosh and A. Agarwal are with the Department of Physics, Indian Institute of Technology Kanpur, India.

S. Bhowmick is with the Department of Material Science and Engineering, Indian Institute of Technology Kanpur, India.

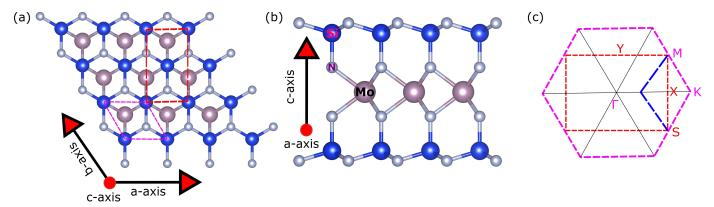


Fig. 1: (a) Top view and (b) side view of ML-MoSi $_2$ N $_4$. The hexagonal primitive cell and orthogonal supercell of ML-MoSi $_2$ N $_4$ are shown by dashed magenta and red lines in (a), respectively. (c) The first Brillouin zone (FBZ) and high symmetry points associated with hexagonal primitive cell (in magenta color) and orthogonal cell (in red color). The blue dashed lines in (c) show the folding of K point associated with FBZ of hexagonal cell to FBZ of orthogonal cell.

Systems (IRDS) 2020 for the year 2034 [38]. The channel length scalability of devices is also studied with their switching performance. Finally, the figure of merits (FOMs) of a combinational circuit (32-bit adder) and a sequential circuit (ALU) are estimated and benchmarked against promising logic technologies (CMOS and beyond-CMOS).

II. COMPUTATIONAL METHODS

Vienna Ab initio Simulation Package (VASP) [39], a tool based on DFT, is used to relax the atomic positions and calculate the electronic structure of ML-MoSi $_2$ N $_4$. The Projector Augmented Wave (PAW) [40] pseudopotentials with planewave basis set are used for DFT calculations. The generalized gradient approximation (GGA) developed by Perdew-Burke-Ernzerhof (PBE) [41] is used to consider exchange and correlation effects. The energy cutoff of 400 eV is used for the plane-wave basis set, and the Brillouin zone integrations are performed using $12 \times 12 \times 1$ k-mesh.

The obtained Bloch/plane-wave states from DFT calculations are mapped to MLWFs using the Wannier90 suite of codes [42]. The obtained TB-like Hamiltonian in MLWF basis is used to construct the Hamiltonian for targeted device dimensions. In the transverse direction (channel width direction), periodic boundary condition (PBC) is considered with 30 uniform wave-vector samples. The constructed device Hamiltonian is used as input to solve coupled Schrödinger and Poisson equations in Non-equilibrium Green's functions (NEGF) formalism [43]–[46]. Additional computational details are described in Appendix.

III. RESULTS

A. Structural and Electrical Properties of ML-MoSi₂N₄

The two dimensional periodic replication of one Mo, two Si, and four N atoms, packed in honey-comb lattice, generate the ML of $\mathrm{MoSi_2N_4}$ (see Fig. 1 (a) and (b)). This ML can be viewed as $\mathrm{MoN_2}$ (2H $-\mathrm{MoS_2}$ like structure) sandwitched between two buckled honeycomb SiN layers (see Fig. 1 (b)). The optimized lattic constant is $a(=b) \sim 2.90$ Å and the thickness of ML is ~ 7.01 Å. The optimized structural parameters agree well with the literature [10], [47], [48].

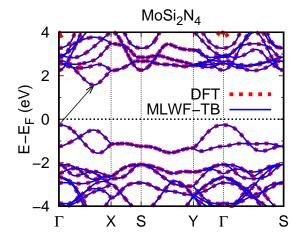
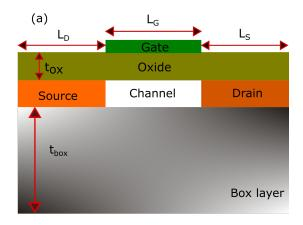


Fig. 2: Electronic band structure of $MoSi_2N_4$ calculated using DFT and MLWF-TB along the high symmetry path.

The electronic band structure of $MoSi_2N_4$ is plotted along with the high symmetry points $(\Gamma\text{-X-S-Y-}\Gamma\text{-S})$ in the orthogonal Brillouin zone (BZ). Figure. 1 (c) shows the BZ associated with hexagonal cell and orthogonal cell. Figure. 2 shows the band structure of $MoSi_2N_4$ obtained from DFT and MLWF-TB Hamiltonian. The band structure from MLWF-TB Hamiltonian shows a good match with DFT near VBM and CBM. It is an indirect band gap semiconductor with the conduction band maxima (CBM) lies in the way from Γ to X (equivalent to K in hexagonal BZ) and valance band maxima (VBM) at Γ . The curvature of CBM and VBM are isotropic, but the curvature of CBM is larger than the curvature of VBM. Hence, larger effective mass for holes (m_h^*) than electrons (m_e^*) i.e., $m_h^* > m_e^*$ (see Table I).

B. Device Structure and Electrical Characteristics

The Single gate (SG) and double-gate (DG) devices, using ML of $MoSi_2N_4$ as channel material, are investigated. Figure. 3 (a) and 3 (b) show the schematic of SG and DG devices, respectively. The geometrical parameters of the devices are gate length (L_G) , channel length (L_{Ch}) , source/drain extension



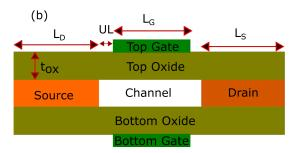


Fig. 3: Schematic of (a) single gate (SG) and (b) double gate (DG) FETs. BOX layer and gate oxides are SiO₂, of thickness t_{box} and t_{ox} , respectively. L_G , UL, and L_{Ch} (= $L_G + 2 \times UL$) are gate length, underlap length, and channel length, respectively. $L_{S/D}$ is source/drain extension length. The source and drain are heavily doped with donors/acceptors for n-/p-type devices. This doping results in the energy degeneracy of 50 meV.

 $L_{S/D}$, underlap length (UL), and oxide thickness (t_{ox}) . For SG, t_{box} is BOX layer thickness with $t_{box}=10\,\mathrm{nm}$. Silicon dioxide (SiO₂) is used as gate oxide and BOX layer. This work aims to assess the intrinsic performance of FETs based on the mono-layer of MoSi₂N₄. Hence, the S/channel/D doping used in the device simulations are n+/undoped (intrinsic)/n+ and p+/undoped (intrinsic)/p+ for n- and p-type devices, respectively. The S/D is doped such that the Fermi level is 50 meV above/below the conduction/valance band for n-FET/p-FET. The metal gate work function is tuned to get $I_{ds} \sim 10^{-2}\,\mu\mathrm{A}/\mu\mathrm{m}$ (say it OFF-current (I_{OFF}) at $V_{gs}=0\,\mathrm{V}$ for all the simulated devices.

We start the investigation by simulating SG and DG devices with $L_{Ch}(=L_G)=12\,\mathrm{nm}$, equivalent oxide thickness (EOT) = 0.60 nm, and $V_{DD}=0.50\,\mathrm{V}$. The source-to-drain tunneling is negligible for the devices with $L_{Ch}=12\,\mathrm{nm}$, and the band-to-band tunneling is negligible due to the high value of band gap in this ML. These device parameters are considered according to IRDS 2020 roadmap for the year 2034. According to the roadmap, the expected channel materials are germanium (Ge) and 2D materials, and the expected devices are 2D materials based devices and FeFETs for the year 2034 [38]. Figure. 4 shows the transfer characteristics for n-FETs and p-FETs. In both types, DG configuration shows a steeper subthreshold slope (SS) and higher I_{ON} than SG.

The SS for thermionic current is proportional to $1 + C_q/C_{OX}$ [49], where C_q is quantum capacitance and C_{OX}

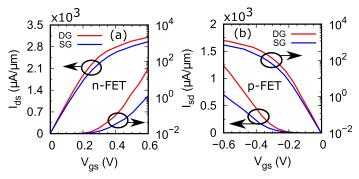


Fig. 4: Transfer characteristics of (a) n-FET and (b) p-FET using MoSi₂N₄ as channel material. $L_{\rm Ch}(=L_{\rm G})=12$ nm, $t_{\rm ox}=0.6$ nm, and $V_{\rm DD}=0.50$ V. The $I_{\rm OFF}$ is fixed at $10^{-2}\mu A/\mu m$ for all devices.

is oxide capacitance. For DG configuration, oxide capacitance is double than SG, hence DG devices show better SS than SG for $L_{Ch}=12\,\mathrm{nm}$. The stepper SS and higher value of C_{OX} in DG ensure higher $d|I_{ds}|/d|V_{gs}|$ and higher mobile carrier concentration, respectively than SG, hence higher I_{ON} than SG. Defects and series parasitics resistance from contacts and S/D access region are not included in our simulations, usually limiting the device's performance.

1) Channel length Scaling: The channel length scaling is performed to study the scalability and immunity to source-to-drain tunneling (SDT) of ML-MoSi₂N₄ based FETs. The SDT plays a significant role in deteriorating device performance at short channel lengths. It is more severe for the low effective mass carriers than high effective mass, as the tunneling probability [50] is proportional to $\exp(-\sqrt{m^*})$. Figures. 5 (a), (b), (c), and (d) show the transfer characteristics of DG n-FET, DG p-FET, SG n-FET, and SG p-FET, respectively for various channel lengths $L_{Ch} = 12, 8, 5, 3$ nm.

The impact of SDT is more for n-type devices than p-type because the curvature of CBM is greater than VBM. For each type, DG is more immune to SDT than SG as DG shows better gate controllability than SG. Hence, DG devices are more scalable than SG. The best scalable device is DG p-FET, and it can be scaled down to 5 nm. At $L_{Ch} = 5$ nm, DG p-FET show SS ~ 65 and $I_{ON}/I_{OFF} > 3 \times 10^6$ for LP applications; For HP applications, it shows SS ~ 67 mV/decade and $I_{ON}/I_{OFF} > 10^4$.

Figure. 6 shows the output characteristics of DG n-FET and p-FET with $L_{Ch} = 5$ nm. Figure. 7 shows I_{ON} and SS of n-FET and p-FET for various L_{Ch} at three different values of I_{OFF} . Also, for a full assessment of DG devices at short channel lengths, DIBL is estimated from the change in threshold voltage (V_{th}) obtained by varying V_{ds} from V_{low} (= 50 mV) to V_{DD} . Figures. 8 (a) and (b) show the variations of SS and DIBL with L_{Ch} , respectively. Figure. 9 shows the variation of I_{ON} vs. L_{Ch} for DG n- and p-FETs based on

TABLE I: Lattice parameters (a(=b)), Electronic Band Gap (E_G) , electron/hole effective mass (m_e^*/m_h^*) and location of CBM/VBM for ML of MoSi₂N₄

| | a (Å) | h(Å) | $E_{G}(eV)$ | m_e^* | m_h^* | VBM/CBM |
|----------------------------------|-------|------|-------------|---------|---------|---------|
| MoSi ₂ N ₄ | 2.90 | 7.01 | 1.842 | 0.478 | 1.184 | Γ / Γ-Χ |

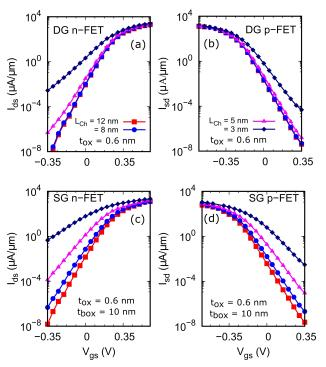


Fig. 5: Transfer characteristics of double gate: (a) n-FET (b) p-FET and single gate: (c) n-FET (d) p-FET for different channel lengths.

ML-MoSi₂N₄ and other promising 2D materials. For both types, the ML-BP FETs show the highest I_{ON} [51], [52] among others (the data is not shown in the figure). But, the stability of BP remains the primary concern [14]. For n-type devices: (1) For $L_{Ch} > 5 \,\mathrm{nm}$, ML-As, and ML- Bi_2O_2Se have high I_{ON} than ML-MoSi₂N₄. However, the preparation of As can produce toxic arsenic trioxide, making its fabrication more complex, other than stability issue [53]. ML-Bi₂O₂Se shows good environmental stability [54]. But the short-channel effects are more in ML-As and ML-Bi₂O₂Se than ML-MoSi₂N₄. (2) ML-InSe shows the lower value of I_{ON} than ML-MoSi₂N₄ and the I_{ON} difference increases as we go below 5 nm channel length. However, compelling surface oxidation in InSe deteriorates mobility and causes uncontrollable current hysteresis in InSe FETs [55]. (3) The ML-MoSi₂N₄ shows superior ON-state current than ML-MoS₂ FETs. For p-type devices: (1) Except InSe, the MoSi₂N₄ shows superior ON-state current than others for $L_{Ch} < 5 \,\mathrm{nm}$.

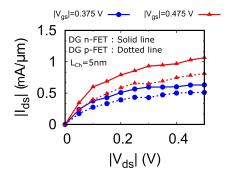


Fig. 6: Output characteristics of DG n-FET and p-FET for $L_{Ch}(=L_{G})=5\ nm.$

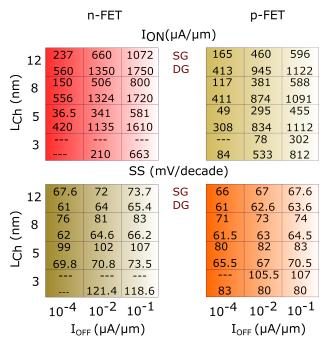
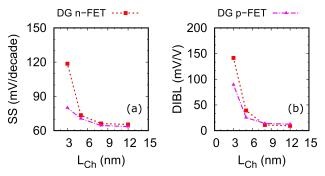


Fig. 7: I_{ON} and sub-threshold swing (SS) of n-FET and p-FET vs L_{Ch} for three different values of I_{OFF} .

- (2) The I_{ON} for ML-MoSi $_2$ N $_4$ is very close to ML-Bi $_2$ O $_2$ Se and superior to others for $L_{Ch} > 5\,\mathrm{nm}$. BL-Bi $_2$ O $_2$ Se suffers from high leakage current due to small bandgap (E $_\mathrm{G} \sim 0.18\,\mathrm{eV}$), and I_{ON} is much lower than ML-MoSi $_2$ N $_4$ for both n- and p-type devices.
- 2) Switching Performance of FETs: The delay and power dissipation product (PDP) are crucial figures of merits (FOMs) for logic applications. They determine switching speed and switching energy (energy per switching event), respectively. Figure. 10 (a) and (b) show the delay $[\tau = (Q_{ON} Q_{OFF})/I_{ON}]$ and PDP $[= (Q_{ON} Q_{OFF})V_{DD}]$ vs L_{Ch} , respectively for DG FETs. These switching parameters for advance Si FETs (Si FinFETs [61], [62] and Si Nanowire FETs [63], [64]) and carbon nanotube (CNT) FETs [65], [66] are also shown in Fig. 10. For MoSi₂N₄ FETs with $L_{Ch} = 3$, 5, 8, 12 nm, τ and PDP lies in range 0.022 0.082 ps and 7.33 51.7 aJ/ μ m, respectively. Overall, MoSi₂N₄ FETs switch faster with lower switching energy than advance Si FETs (0.22 0.48) ps, 55 182 aJ/ μ m) and CNT FETs



 ${\bf Fig.~8:}$ Variation in (a) SS and (b) DIBL for double-gate devices with channel length.

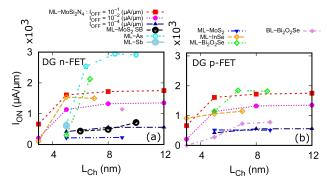


Fig. 9: ON current vs L_{Ch} for DG (a) n-FET and (b) p-FET devices. The data for several promising 2D materials [56]–[59] based DG devices, obtained from first-principle calculations ($I_{OFF}=10^{-1}~\mu\mathrm{A}/\mu\mathrm{m}$), are also shown in same plot for comparison.

 $(0.046-0.184 \text{ ps}, 26-58 \text{ aJ/}\mu\text{m})$. It is worth to notice that the theoretical limit on delay for non-tunneling barrier controlled binary logic switch is 0.04 ps [63]. Our non-tunneling devices $(L_{Ch} = 8 \text{ nm} \text{ and } 12 \text{ nm})$ have τ in the range 0.041-0.082 ps.

The switching performance of DG MoSi $_2$ N $_4$ based FETs ($L_{Ch}=12\,\mathrm{nm}$) is benchmarked against other promising 2D materials based DG FETs [52], [56]–[58]. Other than 1 nm-MoS $_2$ FET, the channel length of other 2D materials based FETs are in the range 7 – 9 nm. The five best performing devices are BP AD n-FET, InSe n-FET, InSe p-FET, MoSi $_2$ N $_4$ n-FET, and MoSi $_2$ N $_4$ p-FET, these have energy-delay product (EDP = PDP $\times \tau$) < (4 \times 10 $^{-30}$ Js/ μ m). The BP armchair direction (AD) n-FET has best switching speed among these, followed by InSe n-FET, InSe p-FET, MoSi $_2$ N $_4$ n-FET, and MoSi $_2$ N $_4$ p-FET. The MoS $_2$ 1nm- L_G FETs have lower switching energy than others, but p-FET and n-FET

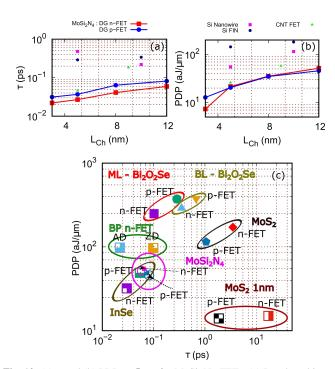
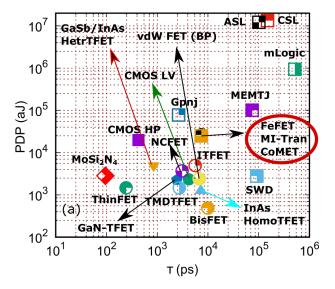


Fig. 10: (a) τ and (b) PDP vs L_{Ch} for MoSi₂N₄ FETs. (c) Benchmarking of MoSi₂N₄ FETs against promising 2D materials based FETs. The performance of 1nm- L_G MoS₂ FET is also shown for comparison.



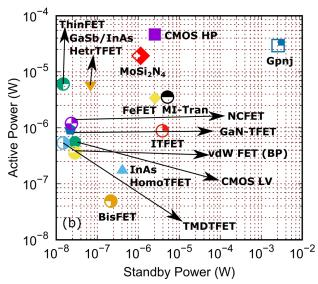


Fig. 11: Comparison of (a) PDP vs τ and (b) active power vs standby power for a 32-bit adder based on ML-MoSi₂N₄ FETs against other promising logic technologies [60].

are ~ 23 times and ~ 212 times slower than MoSi₂N₄ p-FET, respectively. The EDP of our devices are close to high performing InSe p-FET $(2.64\times 10^{-30}~{\rm Js/\mu m})$ and BP AD n-FET $(2.15\times 10^{-30}~{\rm Js/\mu m})$. The best performing device is InSe n-FET with approximately one third EDP than our devices, and EDP of BP zigzag (ZZ) n-FET is approximately three times than our devices. Others (Bi₂O₂Se and MoS₂) have EDP $(25-603\times 10^{-30}~{\rm Js/\mu m})$ far from MoSi₂N₄ FETs. All the devices have $I_{OFF}=10^{-1}~\mu{\rm A/\mu m}$.

3) FOMs of 32-bit Adder and ALU: The FOMs of a combinational (32-bit adder) and a sequential logic circuit (32-bit ALU) based on $MoSi_2N_4$ FETs are estimated, using the methodology of [60], [67]. The n- and p-type DG $MoSi_2N_4$ FETs with $L_{Ch}=12\,\mathrm{nm}$ are considered, and are sized to deliver same current. The 15 nm metal half pitch and 60 nm contacted gate pitch are taken, which results in interconnect capacitance (C_{ic}) = 0.0378 fF and interconnect delay (t_{ic}) = 0.1891 ps for $I_{OFF}=10^{-1}\,\mu\mathrm{A}/\mu\mathrm{m}$ (HP applications).

Using these data, the τ and PDP are calculated for inverter with fan-out of four $(\tau \times PDP = 0.3984 \, ps \times 21.0382 \, aJ)$, NAND gate with fan-in of four $(0.6379 \,\mathrm{ps} \times 19.4914 \,\mathrm{aJ})$, 32-bit adder (111.32 \times 10² ps \times 2.1885 \times 10³ aJ), and ALU $(267.41 \text{ ps} \times 2.2136 \times 10^4 \text{ aJ})$ comprised of MoSi₂N₄ FETs. Figure 11 (a) and 12 (a) show τ vs PDP for 32-bit adder and ALU, respectively based of MoSi₂N₄ and other spintronics and electronics logic devices (these data are taken from [67]). The spintronics devices (ASL, CSL, MEMTJ, mLgic, CoMET, and SWD) based adder and ALU switch slower and consumes more energy than electronics devices. Among electronics devices, switching speed of MoSi₂N₄ based adder and ALU is comparable to CMOS HP and ThinFET (WTe₂/SnSe₂ heterojunction interlayer TFET), but the switching energy of MoSi₂N₄ is one order less than CMOS HP and comparable to TFET devices (ThinFET and GaSb/InAs heterojunction TFET). Further, we characterize the power consumption parameters of adder and ALU. Figures 11 (b) and 12 (b) show the standby power vs. active power for adder and ALU comprised of MoSi₂N₄ FETs and other promising electronic devices. The standby power and active power of the circuits consisting of MoSi₂N₄ devices are close to CMOS HP and more than TFET devices (ThinFET and GaSb/InAs heterojunction TFET).

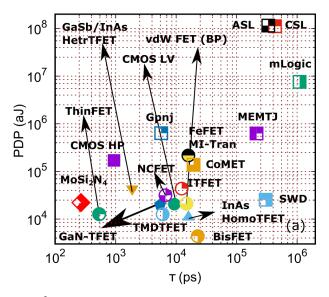
IV. CONCLUSION

Two-dimensional semiconductors are promising candidates as a channel of next-generation electronic devices. In recent years, a new 2D semiconductor with the formula MoSi₂N₄ has been discovered and gaining attention owing to its excellent physical and electronic properties. In this work, the performance of FETs based on recently discovered ML-MoSi₂N₄ is assessed, using the first principles based quantum transport simulations. The upper-performance limit is reported, as the transport is assumed to be ballistic in nature. The scalability and impact of source-to-drain tunneling are investigated by performing channel length scaling study. The double-gate devices are scalable down to 5 nm. However, the p-type devices are more immune to short channel effects (SCEs) than n-type. The performance is estimated as per the IRDS roadmap for the year 2034. The key FOMs for logic switches are calculated and benchmarked against other promising 2D materials-based FETs. It is found that the switching parameters of doublegate devices are better than advanced Si-FETs and CNT-based FETs. Finally, we calculate the FOMs of a combinational and a sequential logic circuit based on our double gate devices and benchmark against CMOS and beyond-CMOS logic technologies. The performance of 32-bit adder and ALU are promising among other alternative logic technologies.

APPENDIX

At each bias (V_{gs}, V_{ds}) , the transmission coefficient can be expressed as,

$$T(E, k, V_{gs}, V_{ds}) = Trace[\Gamma_S G^R \Gamma_D G^A] . \tag{1}$$



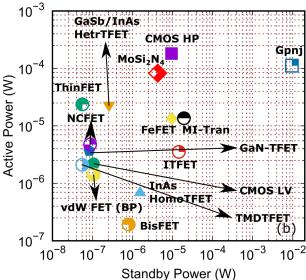


Fig. 12: Comparison of (a) PDP vs τ and (b) active power vs standby power for a 32-bit ALU based on ML-MoSi₂N₄ FETs against other promising logic technologies [60]. The performance of ALU comprised of MoSi₂N₄ FETs is comparable to CMOS-HP.

Here, G^R and G^A are retarded and advance Green functions, respectively. Γ_S/D is the broadening from source/drain contacts. G^R , $\Gamma_{L/R}$, and G^A can be expressed as,

$$G^{R}(E, k, V_{qs}, V_{ds}) = [EI - H(k) - \Sigma]^{-1}$$
, (2a)

$$\Gamma_{S/D}(E, k, V_{qs}, V_{ds}) = i[\Sigma_{S/D} - \Sigma_{S/D}^{\dagger}],$$
 (2b)

$$G^{A}(E, k, V_{gs}, V_{ds}) = [G^{R}(E, k, V_{gs}, V_{ds})]^{\dagger},$$
 (2c)

where, E and I are energy and identity matrix, respectively. Σ (= $\Sigma_S + \Sigma_D$) is the sum of source and drain contact self-energy matrix, and H(k) is the channel Hamiltonian.

Next, the drain current (I_{ds}) is calculated using the Landauer-Büttiker approach [68]. For a given gate-to-source voltage (V_{gs}) and drain-to-source voltage (V_{ds}) , it can be expressed as,

$$I_{ds}(V_{gs}, V_{ds}) = \frac{e}{\pi \hbar} \int_{-\infty}^{\infty} \sum_{k} T(E, k, V_{gs}, V_{ds}) [f(E - \mu_s) - f(E - \mu_d)] dE , \qquad (3)$$

where, e is the electron charge, \hbar is the reduced Planck constant, $T(E,V_{gs},V_{ds}) = \sum_k T(E,k,V_{gs},V_{ds})$ is the transmission coefficient at Energy E for a given bias (V_{gs},V_{ds}) , $\mu_{s/d}$ is the chemical potential at source/drain, and $f(E-\mu_{s/d})$ is the Fermi-Dirac distribution function at source/drain.

REFERENCES

- K. S. Novoselov, A. K. Geim, S. V. Morozov, D. Jiang, Y. Zhang, S. V. Dubonos, I. V. Grigorieva, and A. A. Firsov, "Electric field effect in atomically thin carbon films," *Science*, vol. 306, no. 5696, pp. 666–669, 2004, doi: 10.1126/science.1102896.
- [2] K. S. Novoselov, D. Jiang, F. Schedin, T. J. Booth, V. V. Khotkevich, S. V. Morozov, and A. K. Geim, "Two-dimensional atomic crystals," *Proceedings of the National Academy of Sciences*, vol. 102, no. 30, pp. 10451–10453, 2005, doi: 10.1073/pnas.0502848102.
- [3] K. S. Novoselov, "Nobel lecture: Graphene: Materials in the flatland," Rev. Mod. Phys., vol. 83, pp. 837–849, Aug 2011, doi: 10.1103/RevModPhys.83.837.
- [4] M. Chhowalla, D. Jena, and H. Zhang, "Two-dimensional semiconductors for transistors," *Nature Reviews Materials*, vol. 1, no. 11, p. 16052, Aug 2016, doi: 10.1038/natrevmats.2016.52.
- [5] S. Das, "Two dimensional electrostrictive field effect transistor (2D-EFET): A sub-60mV/decade steep slope device with High ON current," *Scientific Reports*, vol. 6, no. 1, p. 34811, Oct 2016, doi: 10.1038/srep34811.
- [6] C. Qiu, F. Liu, L. Xu, B. Deng, M. Xiao, J. Si, L. Lin, Z. Zhang, J. Wang, H. Guo, H. Peng, and L.-M. Peng, "Dirac-source field-effect transistors as energy-efficient, high-performance electronic switches," vol. 361, no. 6400, pp. 387–392, 2018, doi: 10.1126/science.aap9195.
- [7] N. Oliva, J. Backman, L. Capua, M. Cavalieri, M. Luisier, and A. M. Ionescu, "WSe₂/SnSe₂ vdW heterojunction tunnel FET with subthermionic characteristic and MOSFET co-integrated on same WSe₂ flake," npj 2D Materials and Applications, vol. 4, no. 1, p. 5, Apr 2020, doi: 10.1038/s41699-020-0142-2.
- [8] S. B. Desai, S. R. Madhvapathy, A. B. Sachid, J. P. Llinas, Q. Wang, G. H. Ahn, G. Pitner, M. J. Kim, J. Bokor, C. Hu, H.-S. P. Wong, and A. Javey, "MoS₂ transistors with 1-nanometer gate lengths," vol. 354, no. 6308, pp. 99–102, 2016, doi: 10.1126/science.aah4698.
- [9] Y.-L. Hong, Z. Liu, L. Wang, T. Zhou, W. Ma, C. Xu, S. Feng, L. Chen, M.-L. Chen, D.-M. Sun, X.-Q. Chen, H.-M. Cheng, and W. Ren, "Chemical vapor deposition of layered two-dimensional MoSi₂N₄ materials," vol. 369, no. 6504, pp. 670–674, 2020, doi: 10.1126/science.abb7023.
- [10] A. Bafekry, M. Faraji, D. M. Hoat, M. Shahrokhi, M. M. Fadlallah, F. Shojaei, S. A. H. Feghhi, M. Ghergherehchi, and D. Gogova, "MoSi₂N₄ single-layer: a novel two-dimensional material with outstanding mechanical, thermal, electronic and optical properties," *Journal of Physics D: Applied Physics*, vol. 54, no. 15, p. 155303, feb 2021, doi: 10.1088/1361-6463/abdb6b.
- [11] J. Yu, J. Zhou, X. Wan, and Q. Li, "High intrinsic lattice thermal conductivity in monolayer MoSi₂N₄," *New Journal of Physics*, vol. 23, no. 3, p. 033005, mar 2021, doi: 10.1088/1367-2630/abe8f7.
- [12] B. Mortazavi, B. Javvaji, F. Shojaei, T. Rabczuk, A. V. Shapeev, and X. Zhuang, "Exceptional piezoelectricity, high thermal conductivity and stiffness and promising photocatalysis in two-dimensional MoSi₂N₄ family confirmed by first-principles," *Nano Energy*, vol. 82, p. 105716, 2021, doi: 10.1016/j.nanoen.2020.105716.
- [13] R. Islam, B. Ghosh, C. Autieri, S. Chowdhury, A. Bansil, A. Agarwal, and B. Singh, "Tunable spin polarization and electronic structure of bottom-up synthesized MoSi₂N₄ materials," arXiv preprint arXiv:2105.02739, 2021.
- [14] S. Gamage, Z. Li, V. S. Yakovlev, C. Lewis, H. Wang, S. B. Cronin, and Y. Abate, "Nanoscopy of black phosphorus degradation," *Advanced Materials Interfaces*, vol. 3, no. 12, p. 1600121, 2016, doi: 10.1002/admi.201600121.
- [15] S. Ross and A. Sussman, "Surface oxidation of molybdenum disulfide," The Journal of Physical Chemistry, vol. 59, no. 9, pp. 889–892, 1955, doi: 10.1021/j150531a020.

- [16] B. Radisavljevic, A. Radenovic, J. Brivio, V. Giacometti, and A. Kis, "Single-layer MoS₂ transistors," *Nature Nanotechnology*, vol. 6, no. 3, pp. 147–150, Mar 2011, doi: 10.1038/nnano.2010.279.
- [17] A. Nourbakhsh, A. Zubair, R. N. Sajjad, A. Tavakkoli K. G., W. Chen, S. Fang, X. Ling, J. Kong, M. S. Dresselhaus, E. Kaxiras, K. K. Berggren, D. Antoniadis, and T. Palacios, "MoS₂ field-effect transistor with sub-10 nm channel length," *Nano Letters*, vol. 16, no. 12, pp. 7798–7806, 2016, doi: 10.1021/acs.nanolett.6b03999.
- [18] F. Zhang and J. Appenzeller, "Tunability of short-channel effects in MoS₂ field-effect devices," *Nano Letters*, vol. 15, no. 1, pp. 301–306, 2015, doi: 10.1021/nl503586v.
- [19] I. Lee, J. N. Kim, W. T. Kang, Y. S. Shin, B. H. Lee, and W. J. Yu, "Schottky barrier variable graphene/multilayer-MoS₂ heterojunction transistor used to overcome short channel effects," ACS Applied Materials & Interfaces, vol. 12, no. 2, pp. 2854–2861, 2020, doi: 10.1021/acsami.9b18577.
- [20] D. Sarkar, W. Liu, X. Xie, A. C. Anselmo, S. Mitragotri, and K. Banerjee, "MoS₂ field-effect transistor for next-generation labelfree biosensors," ACS Nano, vol. 8, no. 4, pp. 3992–4003, 2014, doi: 10.1021/nn5009148.
- [21] W. Liu, D. Sarkar, J. Kang, W. Cao, and K. Banerjee, "Impact of contact on the operation and performance of back-gated monolayer MoS₂ fieldeffect-transistors," ACS Nano, vol. 9, no. 8, pp. 7904–7912, 2015, doi: 10.1021/nn506512j.
- [22] X. Xie, D. Sarkar, W. Liu, J. Kang, O. Marinov, M. J. Deen, and K. Banerjee, "Low-frequency noise in bilayer MoS₂ transistor," ACS Nano, vol. 8, no. 6, pp. 5633–5640, 2014, doi: 10.1021/nn4066473.
- [23] B. Chakraborty, A. Bera, D. V. S. Muthu, S. Bhowmick, U. V. Waghmare, and A. K. Sood, "Symmetry-dependent phonon renormalization in monolayer MoS₂ transistor," *Phys. Rev. B*, vol. 85, p. 161403, Apr 2012, doi: 10.1103/PhysRevB.85.161403.
- [24] Y. Yoon, K. Ganapathi, and S. Salahuddin, "How good can monolayer MoS₂ transistors be?" *Nano Letters*, vol. 11, no. 9, pp. 3768–3773, 2011, doi: 10.1021/nl2018178.
- [25] P. Rastogi, S. Kumar, S. Bhowmick, A. Agarwal, and Y. S. Chauhan, "Doping strategies for monolayer MoS₂ via surface adsorption: A systematic study," *The Journal of Physical Chemistry C*, vol. 118, no. 51, pp. 30 309–30 314, Dec 2014, doi: 10.1021/jp510662n.
- [26] C. Yadav, A. Agarwal, and Y. S. Chauhan, "Compact modeling of transition metal dichalcogenide based thin body transistors and circuit validation," *IEEE Transactions on Electron Devices*, vol. 64, no. 3, pp. 1261–1268, 2017, doi: 10.1109/TED.2016.2643698.
- [27] C. Yadav, P. Rastogi, T. Zimmer, and Y. S. Chauhan, "Charge-based modeling of transition metal dichalcogenide transistors including ambipolar, trapping, and negative capacitance effects," *IEEE Transactions* on *Electron Devices*, vol. 65, no. 10, pp. 4202–4208, 2018, doi: 10.1109/TED.2018.2855109.
- [28] K. Nandan, C. Yadav, P. Rastogi, A. Toral-Lopez, A. Marin-Sanchez, E. G. Marin, F. G. Ruiz, S. Bhowmick, and Y. S. Chauhan, "Compact modeling of multi-layered MoS₂ FETs including negative capacitance effect," *IEEE Journal of the Electron Devices Society*, vol. 8, pp. 1177– 1183, 2020, doi: 10.1109/JEDS.2020.3021031.
- [29] B. Peng, D. Zhang, H. Zhang, H. Shao, G. Ni, Y. Zhu, and H. Zhu, "The conflicting role of buckled structure in phonon transport of 2D group-IV and group-V materials," *Nanoscale*, vol. 9, pp. 7397–7407, 2017, doi: 10.1039/C7NR00838D.
- [30] G. Qin, Q.-B. Yan, Z. Qin, S.-Y. Yue, M. Hu, and G. Su, "Anisotropic intrinsic lattice thermal conductivity of phosphorene from first principles," *Phys. Chem. Chem. Phys.*, vol. 17, pp. 4854–4858, 2015, doi: 10.1039/C4CP04858J.
- [31] W. Li, J. Carrete, and N. Mingo, "Thermal conductivity and phonon linewidths of monolayer MoS₂ from first principles," *Applied Physics Letters*, vol. 103, no. 25, p. 253103, 2013, doi: 10.1063/1.4850995.
- [32] B. D. Kong, S. Paul, M. B. Nardelli, and K. W. Kim, "First-principles analysis of lattice thermal conductivity in monolayer and bilayer graphene," *Phys. Rev. B*, vol. 80, p. 033406, Jul 2009, doi: 10.1103/PhysRevB.80.033406.
- [33] Q. Wang, L. Cao, S.-J. Liang, W. Wu, G. Wang, C. H. Lee, W. L. Ong, H. Y. Yang, L. K. Ang, S. A. Yang, and Y. S. Ang, "Efficient ohmic contacts and built-in atomic sublayer protection in MoSi₂N₄ and WSi₂N₄ monolayers," npj 2D Materials and Applications, vol. 5, no. 1, p. 71, Aug 2021, doi: 10.1038/s41699-021-00251-y.
- [34] Q. Wu, L. Cao, Y. S. Ang, and L. K. Ang, "Semiconductor-to-metal transition in bilayer MoSi₂N₄ and WSi₂N₄ with strain and electric field," *Applied Physics Letters*, vol. 118, no. 11, p. 113102, 2021, doi: 10.1063/5.0044431.

- [35] I. Souza, N. Marzari, and D. Vanderbilt, "Maximally localized Wannier functions for entangled energy bands," *Phys. Rev. B*, vol. 65, p. 035109, Dec 2001, doi: 10.1103/PhysRevB.65.035109.
- [36] Y.-S. Lee, M. B. Nardelli, and N. Marzari, "Band structure and quantum conductance of nanostructures from maximally localized Wannier functions: The case of functionalized carbon nanotubes," *Phys. Rev. Lett.*, vol. 95, p. 076804, Aug 2005, doi: 10.1103/PhysRevLett.95.076804.
- [37] N. Marzari, A. A. Mostofi, J. R. Yates, I. Souza, and D. Vanderbilt, "Maximally localized Wannier functions: Theory and applications," *Rev. Mod. Phys.*, vol. 84, pp. 1419–1475, Oct 2012, doi: 10.1103/RevMod-Phys.84.1419.
- [38] IRDS 2020: https://irds.ieee.org/editions/2020.
- [39] G. Kresse and J. Furthmüller, "Efficient iterative schemes for ab initio total-energy calculations using a plane-wave basis set," *Phys. Rev. B*, vol. 54, pp. 11 169–11 186, Oct 1996, doi: 10.1103/PhysRevB.54.11169.
- [40] P. E. Blöchl, "Projector augmented-wave method," *Phys. Rev. B*, vol. 50, pp. 17 953–17 979, Dec 1994, doi: 10.1103/PhysRevB.50.17953.
- [41] J. P. Perdew, K. Burke, and M. Ernzerhof, "Generalized gradient approximation made simple," *Phys. Rev. Lett.*, vol. 77, pp. 3865–3868, Oct 1996, doi: 10.1103/PhysRevLett.77.3865.
- [42] A. A. Mostofi, J. R. Yates, G. Pizzi, Y.-S. Lee, I. Souza, D. Vanderbilt, and N. Marzari, "An updated version of Wannier90: A tool for obtaining maximally-localised Wannier functions," *Computer Physics Communications*, vol. 185, no. 8, pp. 2309 2310, 2014, doi: 10.1016/j.cpc.2014.05.003.
- [43] S. Datta, Quantum transport: atom to transistor. Cambridge university press, 2005.
- [44] P. Rastogi, T. Dutta, S. Kumar, A. Agarwal, and Y. S. Chauhan, "Quantum confinement effects in extremely thin body germanium n-MOSFETs," *IEEE Transactions on Electron Devices*, vol. 62, no. 11, pp. 3575–3580, 2015, doi: 10.1109/TED.2015.2477471.
- [45] T. Dutta, P. Kumar, P. Rastogi, A. Agarwal, and Y. S. Chauhan, "Atomistic study of band structure and transport in extremely thin channel InP MOSFETs," *physica status solidi* (a), vol. 213, no. 4, pp. 898–904, 2016, doi: 10.1002/pssa.201532727.
- [46] K. Nandan, A. Agarwal, S. Bhowmick, and Y. S. Chauhan, "Performance investigation of p-FETs based on highly air-stable monolayer pentagonal PdSe₂," *IEEE Transactions on Electron Devices*, pp. 1–7, 2021, doi: 10.1109/TED.2021.3119552.
- [47] S. Li, W. Wu, X. Feng, S. Guan, W. Feng, Y. Yao, and S. A. Yang, "Valley-dependent properties of monolayer MoSi₂N₄, WSi₂N₄, and MoSi₂As₄," *Phys. Rev. B*, vol. 102, p. 235435, Dec 2020, doi: 10.1103/PhysRevB.102.235435.
- [48] Y.-L. Hong, Z. Liu, L. Wang, T. Zhou, W. Ma, C. Xu, S. Feng, L. Chen, M.-L. Chen, D.-M. Sun, X.-Q. Chen, H.-M. Cheng, and W. Ren, "Chemical vapor deposition of layered two-dimensional MoSi₂N₄ materials," *Science*, vol. 369, no. 6504, pp. 670–674, 2020, doi: 10.1126/science.abb7023.
- [49] M. Lundstrom and J. Guo, Nanoscale transistors: device physics, modeling and simulation. Springer Science & Business Media, 2006.
- [50] D. J. Griffiths and D. F. Schroeter, *Introduction to quantum mechanics*. Cambridge University Press, 2018.
- [51] D. Yin and Y. Yoon, "Can bilayer black phosphorus outperform monolayer in field-effect transistors?" in 2015 73rd Annual Device Research Conference (DRC), ser. 2015 73rd Annual Device Research Conference (DRC), 2015, doi: 10.1109/DRC.2015.7175614. . ISSN 1548-3770 pp. 177–178
- [52] F. Liu, Y. Wang, X. Liu, J. Wang, and H. Guo, "Ballistic transport in monolayer black phosphorus transistors," *IEEE Transactions on Electron Devices*, vol. 61, no. 11, pp. 3871–3876, 2014, doi: 10.1109/TED.2014.2353213.
- [53] S. Zhang, S. Guo, Z. Chen, Y. Wang, H. Gao, J. Gómez-Herrero, P. Ares, F. Zamora, Z. Zhu, and H. Zeng, "Recent progress in 2D group-VA semiconductors: from theory to experiment," *Chem. Soc. Rev.*, vol. 47, pp. 982–1021, 2018, doi: 10.1039/C7CS00125H.
- [54] J. Wu, H. Yuan, M. Meng, C. Chen, Y. Sun, Z. Chen, W. Dang, C. Tan, Y. Liu, J. Yin, Y. Zhou, S. Huang, H. Q. Xu, Y. Cui, H. Y. Hwang, Z. Liu, Y. Chen, B. Yan, and H. Peng, "High electron mobility and quantum oscillations in non-encapsulated ultrathin semiconducting Bi₂O₂Se," *Nature Nanotechnology*, vol. 12, no. 6, pp. 530–534, Jun 2017, doi: 10.1038/nnano.2017.43.
- [55] P.-H. Ho, Y.-R. Chang, Y.-C. Chu, M.-K. Li, C.-A. Tsai, W.-H. Wang, C.-H. Ho, C.-W. Chen, and P.-W. Chiu, "High-mobility InSe transistors: The role of surface oxides," ACS Nano, vol. 11, no. 7, pp. 7362–7370, 2017, doi: 10.1021/acsnano.7b03531.
- [56] R. Quhe, J. Liu, J. Wu, J. Yang, Y. Wang, Q. Li, T. Li, Y. Guo, J. Yang, H. Peng, M. Lei, and J. Lu, "High-performance sub-10 nm

- monolayer $\mathrm{Bi}_2\mathrm{O}_2\mathrm{Se}$ transistors," *Nanoscale*, vol. 11, pp. 532–540, 2019, doi: 10.1039/C8NR08852G.
- [57] Y. Wang, R. Fei, R. Quhe, J. Li, H. Zhang, X. Zhang, B. Shi, L. Xiao, Z. Song, J. Yang, J. Shi, F. Pan, and J. Lu, "Many-body effect and device performance limit of monolayer InSe," ACS Applied Materials & Interfaces, vol. 10, no. 27, pp. 23344–23352, 2018, doi: 10.1021/acsami.8b06427.
- [58] J. Yang, R. Quhe, Q. Li, S. Liu, L. Xu, Y. Pan, H. Zhang, X. Zhang, J. Li, J. Yan, B. Shi, H. Pang, L. Xu, Z. Zhang, J. Lu, and J. Yang, "Sub 10 nm bilayer Bi₂O₂Se transistors," *Advanced Electronic Materials*, vol. 5, no. 3, p. 1800720, 2019, doi: https://doi.org/10.1002/aelm.201800720.
- [59] Y. Wang, P. Huang, M. Ye, R. Quhe, Y. Pan, H. Zhang, H. Zhong, J. Shi, and J. Lu, "Many-body effect, carrier mobility, and device performance of hexagonal arsenene and antimonene," *Chemistry of Materials*, vol. 29, no. 5, pp. 2191–2201, 2017, doi: 10.1021/acs.chemmater.6b04909.
- [60] D. E. Nikonov and I. A. Young, "Benchmarking of beyond-cmos exploratory devices for logic integrated circuits," *IEEE Journal on Exploratory Solid-State Computational Devices and Circuits*, vol. 1, pp. 3–11, 2015, doi: 10.1109/JXCDC.2015.2418033.
- [61] D. A. Antoniadis, I. Aberg, C. N. Chleirigh, O. M. Nayfeh, A. Khakifirooz, and J. L. Hoyt, "Continuous MOSFET performance increase with device scaling: The role of strain and channel material innovations," *IBM Journal of Research and Development*, vol. 50, no. 4.5, pp. 363–376, 2006, doi: 10.1147/rd.504.0363.
- [62] B. Doris, M. Ieong, T. Zhu, Y. Zhang, M. Steen, W. Natzle, S. Callegari, V. Narayanan, J. Cai, S. H. Ku, P. Jamison, Y. Li, Z. Ren, V. Ku, T. Boyd, T. Kanarsky, C. D'Emic, M. Newport, D. Dobuzinsky, S. Deshpande, J. Petrus, R. Jammy, and W. Haensch, "Device design considerations for ultra-thin SOI MOSFETs," in *IEEE International Electron Devices Meeting 2003*, ser. IEEE International Electron Devices Meeting 2003, doi: 10.1109/IEDM.2003.1269360. pp. 27.3.1–27.3.4.
- [63] R. W. Keyes, "Fundamental limits in digital information processing," Proceedings of the IEEE, vol. 69, no. 2, pp. 267–278, 1981, doi: 10.1109/PROC.1981.11959.
- [64] H. Iwai, "End of the scaling theory and Moore's law," in 2016 16th International Workshop on Junction Technology (IWJT), ser. 2016 16th International Workshop on Junction Technology (IWJT), 2016, doi: 10.1109/IWJT.2016.7486661. pp. 1–4.
- [65] S. E. Thompson and S. Parthasarathy, "Moore's law: the future of Si microelectronics," *Materials Today*, vol. 9, no. 6, pp. 20–25, 2006, doi: 10.1016/S1369-7021(06)71539-5.
- [66] A. Javey, J. Guo, Q. Wang, M. Lundstrom, and H. Dai, "Ballistic carbon nanotube field-effect transistors," *Nature*, vol. 424, no. 6949, pp. 654– 657, Aug 2003, doi: 10.1038/nature01797.
- [67] C. Pan and A. Naeemi, "An expanded benchmarking of beyond-CMOS devices based on boolean and neuromorphic representative circuits," *IEEE Journal on Exploratory Solid-State Computational Devices and Circuits*, vol. 3, pp. 101–110, 2017, doi: 10.1109/JXCDC.2018.2793536.
- [68] M. Büttiker, Y. Imry, R. Landauer, and S. Pinhas, "Generalized many-channel conductance formula with application to small rings," *Phys. Rev. B*, vol. 31, pp. 6207–6215, May 1985, doi: 10.1103/PhysRevB.31.6207.